

Spectroscopy and photon echo at the Er^{3+} transition with a small inhomogeneous broadening and telecommunication wavelength in a YPO_4 crystal

© K.I. Gerasimov¹, T.N. Sabirov¹, S.A. Moiseev¹, E.I. Baibekov², M. Bettinelli³,
M.S. Chou⁴, Y.-C. Yen⁴, M.N. Popova⁵

¹Kazan Quantum Center, Kazan National Research Technical University named after A.N. Tupolev – KAI,
420111 Kazan, Russia

²Kazan (Volga Region) Federal University, 420008 Kazan, Russia

³Dipartimento di Biotecnologie, University of Verona and INSTM,
37134 Verona, Italy

⁴Department of Materials and Optoelectronic Science, Center of Crystal Research, National Sun Yat-Sen University,
80424 Kaohsiung, Taiwan

⁵Institute of Spectroscopy, Russian Academy of Sciences, Troitsk, Moscow, Russia

E-mail: kigerasimov@mail.ru

Received November 08, 2022

Revised November 08, 2022

Accepted December 06, 2022

The results of investigations of Er^{3+} ions at an optical transition with a telecommunication wavelength ($\lambda \sim 1530$ nm) in a YPO_4 crystal by using photon echo and high-resolution laser spectroscopy in magnetic fields up to 4 T are presented. The maximum coherence time (T_2) was 113 μs in a magnetic field of 4 T when it is oriented along the optical axis c of the crystal. The main sources of decoherence are discussed.

Keywords: $\text{YPO}_4:\text{Er}$ crystals, photon echo, high-resolution laser spectroscopy, magnetic field.

DOI: 10.61011/EOS.2023.05.56513.69-22

Introduction

Dielectric crystals activated by rare-earth ions (REI) are widely used as laser materials, scintillators, phosphors, and optical radiation converters. Recently, REI in crystals are considered as one of the most promising systems for quantum information technologies [1–6]. The reason for the increased interest in REI is the large coherence (phase relaxation) time for both optical and electron-nuclear spin transitions. The most promising from this point are oxide crystals [7,8], where the nearest environment of REI are oxygen ions, for which the natural abundance of ^{17}O isotopes with nonzero nuclear spin is very low (0.038%). Due to this, the flip-flop transitions of the nuclear spins of oxygen ions, which cause fluctuations of the local magnetic field on the REI and determine one of the main mechanisms of decoherence in the REI system, are significantly suppressed. A striking example of such suppression of the influence of local magnetic field fluctuations is the achievement of record coherence times of Eu^{3+} and Er^{3+} for optical (2.6 ms [9] and 4.4 ms [10,11], respectively) and electron-nuclear spin (6 h [2] and 1 s [12], respectively) transitions in orthosilicate crystals Y_2SiO_5 .

In the REI series, only the Er^{3+} ion has a long-lived excited state with an optical transition at the telecommunication wavelength ($\sim 1.5 \mu\text{m}$). This feature of Er^{3+} in crystals makes this ion particularly promising

for creating an optical quantum memory (QM) and a quantum repeater [13] on its basis for implementing long-range quantum communications [14–17]. Recently, it has also been proposed to use the Er^{3+} ion for quantum processing in a scalable platform of nano-optical resonant cavities [18–21]. Thus, the search and study of new oxide crystals activated by Er^{3+} is an urgent task for the creation of promising QM materials and quantum processing.

We have recently measured the high-resolution luminescence and absorption spectra of $\text{YPO}_4:\text{Er}^{3+}$ single crystals, determined the reliable parameters of the crystal field, and deciphered the hyperfine structure of the absorption spectra associated with the odd isotope $^{167}\text{Er}^{3+}$ [22]. In this paper, we present the results of studies of the optical transition $^4I_{15/2}(\Gamma_7^1) \rightarrow ^4I_{13/2}(\Gamma_6^1)$ in $\text{Er}^{3+}:\text{YPO}_4$ ($\lambda \sim 1530$ nm) in magnetic fields up to 4 T, using high-resolution laser spectroscopy and photon echo methods. For one of the crystals, we observed relatively narrow absorption lines (~ 70 MHz), which makes this crystal promising for studying the hyperfine structure of optical transitions. According to our data, we present the first experimental results on the optical coherence times for $\text{Er}^{3+}:\text{YPO}_4$ at these transitions and their dependence on the strength of the external magnetic field. In conclusion, the results obtained and the prospects for using $\text{YPO}_4:\text{Er}^{3+}$ crystals in quantum devices are discussed.

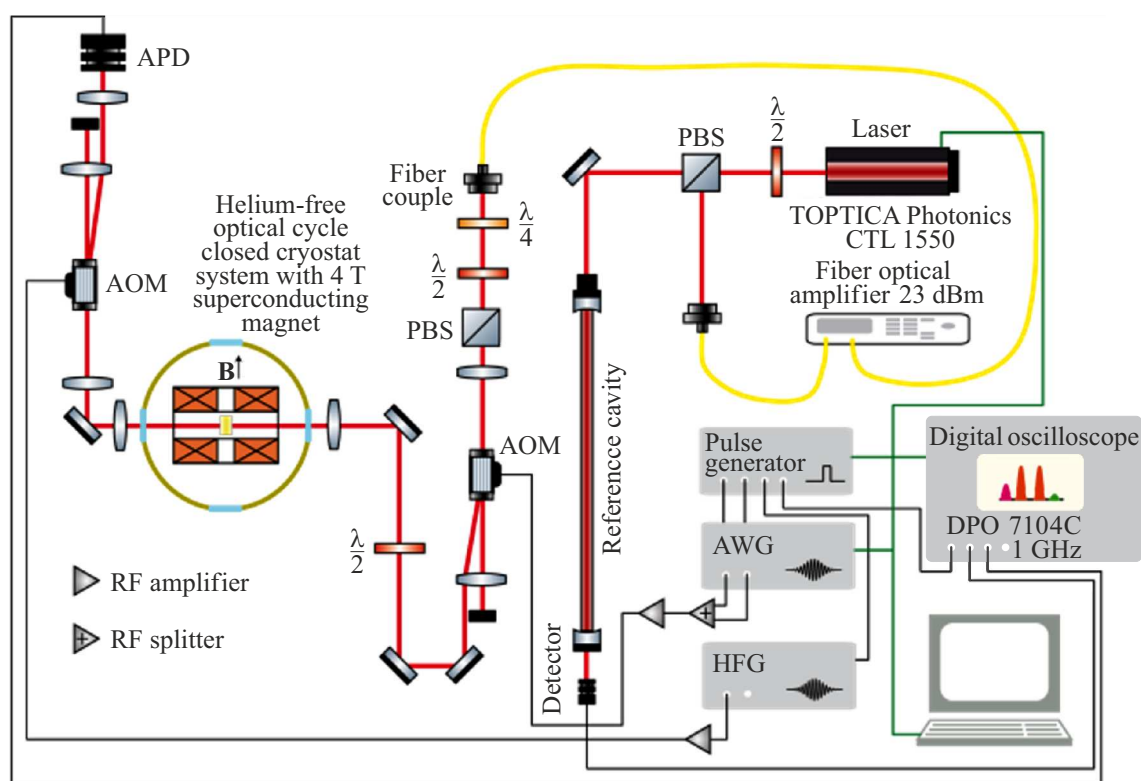


Figure 1. Simplified diagram of the experimental setup for high-resolution laser spectroscopy and photon echo. APD — avalanche photodiode, PBS — polarizing beam splitter, AOM — acousto-optical modulator, AWG — arbitrary waveform generator, HFG — high frequency generator.

Experiment details

Three $\text{YPO}_4:\text{Er}^{3+}$ samples (S1, S2 and S3) with nominal concentrations of erbium ions ~ 0.1 (S1), 0.01 (S2), and 0.005 at.% (S3) were under study. The samples were grown in two laboratories at different times. The crystal growth method is described in the previous paper [22]. The crystals were in the form of thin plates with sizes $2 \times 1 \times 0.24$, $6 \times 2 \times 0.27$, and $3.7 \times 1.7 \times 0.28$ mm for S1, S2, and S3, respectively. The direction of the crystallographic axis c coincided with the longest edge of the crystal.

The simplified diagram of the experimental setup is shown in Fig. 1. A tunable single-mode single-frequency diode laser (CTL 1500 — TOPTICA Photonics AG) was used as a light source. The frequency scanning of the laser radiation was controlled using a reference resonant cavity. In photon echo experiments, laser pulses were prepared by modulating the intensity of stationary laser radiation using an acousto-optical modulator (AOM). The samples were cooled in a closed cycle optical cryostat with a superconducting magnet. The sample was kept in vacuum and cooled by contact with a cold sample holder. The temperature in all the experiments was 1.3 K. Since the samples were thin plates, in a number of experiments for one or another sample, there was a distortion of the line shape, which we associate with the deformation of the sample during cooling

due to unsuccessful gluing of the sample to a cold holder, as was shown, for example, in the paper [23]. Further, in the results of the paper, data are given when there was either no deformation distortion (samples S1 and S2) or it was minimal (sample S3). Unfortunately, it was not possible to obtain data for sample S3 when there was no deformation at all. Transmittance spectra and photon echo signals were recorded with an APD110C/M avalanche photodiode (Thorlabs) and a DPO7104C digital oscilloscope.

Results and discussion

A. High-resolution laser magneto-optical spectroscopy

A simplified diagram of the energy levels of Er^{3+} ions in YPO_4 crystal is shown in Fig. 2. The ${}^4I_{15/2}(\Gamma_7^1) \rightarrow {}^4I_{13/2}(\Gamma_6^1)$ transition was studied in order to measure the inhomogeneous and homogeneous broadening. The first excited state (Γ_6^1) in the ground multiplet ${}^4I_{15/2}$ has a sufficiently high energy (31 cm^{-1}) and, therefore, has little effect on the homogeneous linewidth of the ${}^4I_{15/2}(\Gamma_7^1) \rightarrow {}^4I_{13/2}(\Gamma_6^{\text{ex}})$ transition at temperatures below 3–4 K (see the discussion in subsection B). The opposite case takes place for the ${}^4I_{13/2}$ multiplet, where the energy difference between the Γ_6^1 and Γ_7^1 states is quite small

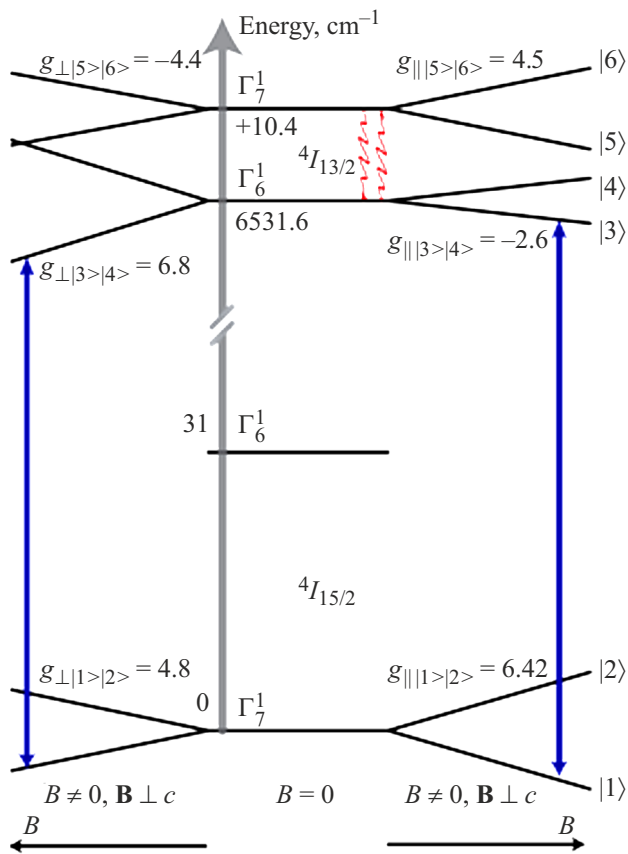


Figure 2. Energy level diagram of the Er^{3+} ion in an YPO_4 single crystal at $B = 0$ and at two orientations of \mathbf{B} . The blue arrows show the transitions at which the phase relaxation time was measured. Red wavy arrows indicate a possible direct relaxation process.

(10.4 cm^{-1}), which can affect the coherence time due to single-quantum transitions that determine direct relaxation processes [24]. For simplicity, we have numbered the studied quantum states from $|1\rangle$ to $|6\rangle$, see the right part of Fig. 2.

In the absorption spectrum of the S1 sample at the ${}^4I_{15/2}(\Gamma_7^1) \rightarrow {}^4I_{13/2}(\Gamma_6^1)$ transition, a very intense line was observed with a relatively large spectral width of approximately 600 MHz (FWHM) with an absorption coefficient α at a maximum of $\sim 110 \text{ cm}^{-1}$ for $\mathbf{E} \perp c$ (\mathbf{E} is the electric field vector of laser radiation) and over 200 cm^{-1} for $\mathbf{E} \parallel c$ (this value cannot be measured more accurately using our technique). The linewidths of the central peaks corresponding to the even Er isotopes of the S2 and S3 samples are quite small and amount to approximately 190 and 220 MHz, respectively. We attribute the greater broadening of the line of the sample S3 compared to S2 to the slight deformation of the sample upon cooling. The absorption coefficient at the maximum for samples S2 (S3) is still high, it was 25 (7) cm^{-1} and 96 (29) cm^{-1} for $\mathbf{E} \perp c$ and $\mathbf{E} \parallel c$, respectively. The ratio of the integral absorption coefficient $\int \alpha(\nu) d\nu$ in the frequency range

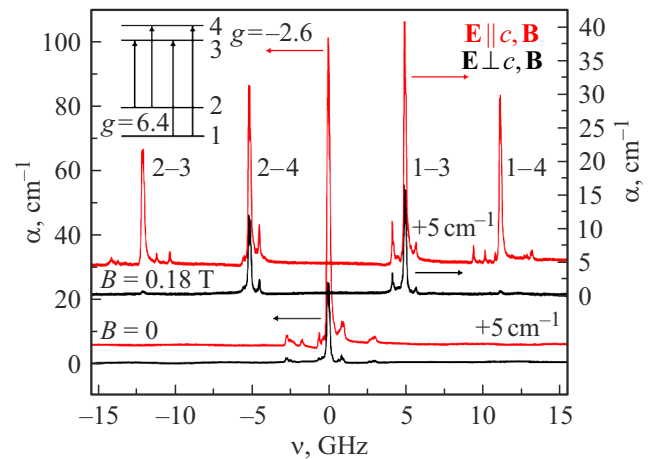


Figure 3. Absorption spectra of $\text{YPO}_4:\text{Er}^{3+}$ ($c = 0.01$ at.%, sample S2, see text) at $T = 1.3 \text{ K}$ and magnetic field $B = 0$ and 0.18 T . Spectra with light polarization $\mathbf{E} \perp c, \mathbf{B}$ and $\mathbf{E} \parallel c, \mathbf{B}$ are shown by black and red lines, respectively. The spectra with polarization $\mathbf{E} \parallel c, \mathbf{B}$ are shifted upward by 5 cm^{-1} for clarity. The center line ($\nu = 0$) at $B = 0$ corresponds to a frequency of 195.812 THz ($\lambda \sim 1531.02 \text{ nm}$). The insert in the upper left corner shows a simplified energy level diagram ($B > 0$) and transitions between two Kramers doublets. The lines in the experimental spectra are marked with the corresponding numbers of the initial and final states of the transitions.

8 GHz ($\mathbf{E} \perp c$) of three samples is $95:8:3$ ($\text{GHz} \cdot \text{cm}^{-1}$), which approximately corresponds to the ratio of erbium concentrations in the samples S1–S3.

In an external magnetic field, the line splits into two ($\mathbf{E} \perp c \parallel \mathbf{B}, \mathbf{E} \parallel c \perp \mathbf{B}, \mathbf{E} \perp c \perp \mathbf{B}$) or four ($\mathbf{E} \parallel c \parallel \mathbf{B}$) components, depending on the polarization of the laser radiation and the direction of the magnetic field relative to the c axis. The dependence of the line splitting on the magnetic field below 1 T is well described by the level shifts determined by the g factors of the ground and excited states [22].

As mentioned earlier, the absorption spectrum of sample S2 differed radically from the absorption spectrum of sample S1 with narrower lines. Fig. 3 shows this spectrum at a temperature of 1.3 K at both zero and 0.18 T magnetic field. In the absence of an external magnetic field, the absorption spectrum of the transition between the ground Kramers doublet $\Gamma_7^1({}^4I_{15/2})$ and the lower doublet (Γ_6^1) in the ${}^4I_{13/2}$ multiplet consists of an intense broad ($\sim 193 \text{ MHz}$) absorption line (absorption coefficient at the maximum $\sim 95 \text{ cm}^{-1}$ for $\mathbf{E} \parallel c, \mathbf{B}$), which corresponds to even isotopes of erbium, and weaker ${}^{167}\text{Er}$ Lorentzian lines with linewidths $70\text{--}80 \text{ MHz}$. Five even Er isotopes in total have the highest percentage in natural abundance (0.14% — ${}^{162}\text{Er}$, 1.6% — ${}^{164}\text{Er}$, 33.6% — ${}^{166}\text{Er}$, 26.8% — ${}^{168}\text{Er}$ and 14.9% — ${}^{170}\text{Er}$, total $\sim 77.1\%$) compared with the isotope ${}^{167}\text{Er}$ ($\sim 22.9\%$). The large linewidth of the even isotopes is due to the unresolved isotopic structure and overlap with the lines of the ${}^{167}\text{Er}$ ion.

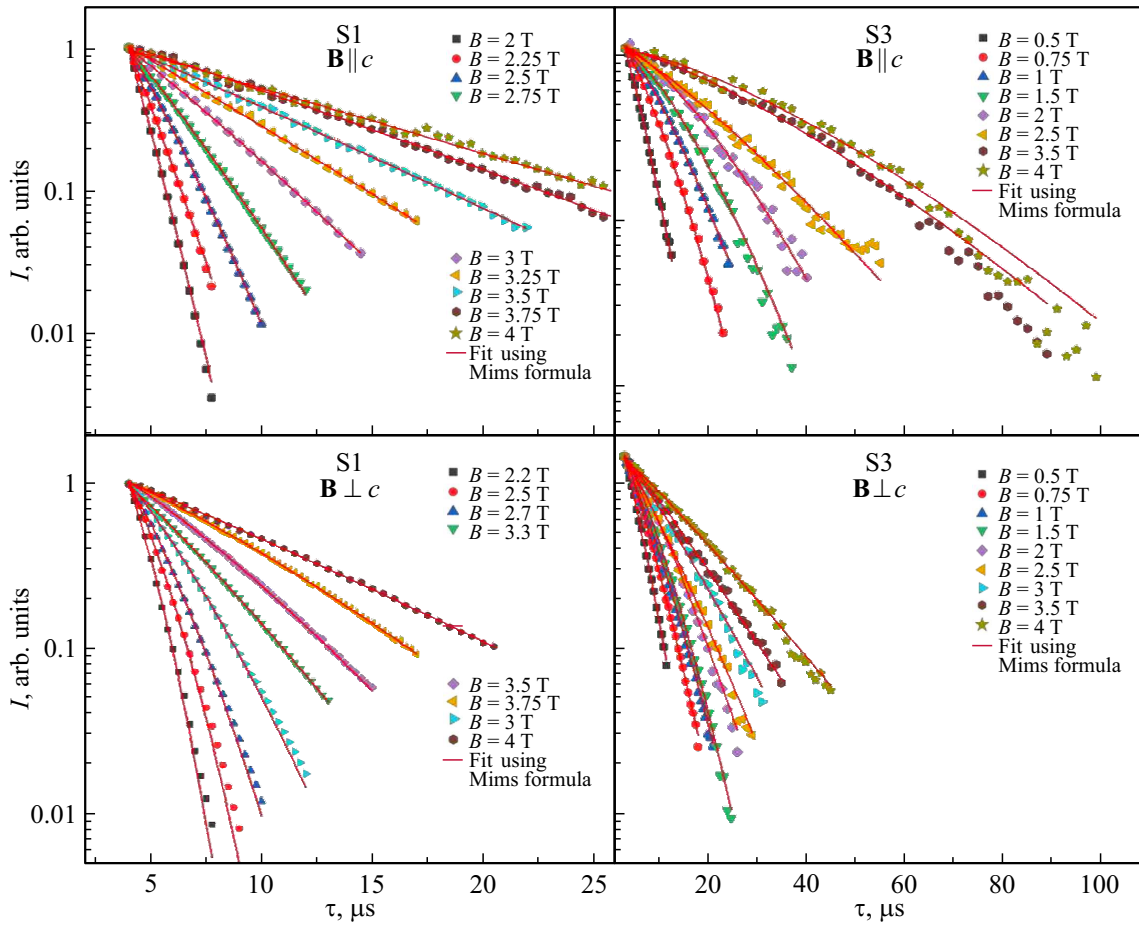


Figure 4. Decay of the two-pulse photon echo in YPO₄: Er³⁺ (samples S1 and S3) at different magnitudes and orientations of the magnetic field. The upper part — $\mathbf{B} \parallel c$, the lower part — $\mathbf{B} \perp c$. The horizontal axis shows the delay time τ between two excitation pulses. Red curves — approximation of the results using the Mims formula.

B. Photon echo

For samples S1 and S3, the dependences of the phase relaxation time on the magnetic field were measured. The first crystal has a high absorbance, which is of interest for some quantum memory protocols, such as AFC or GEM. The second crystal has the lowest concentration and is interesting from the standpoint of obtaining the longest phase relaxation times. Preliminary studies of the S2 sample showed that in the maximum magnetic field (4 T) the phase relaxation time was shorter than that of the S3 sample, and the detailed field dependence for S2 was not measured.

In sample S1, the photon echo signals had a sufficiently high intensity when measured in magnetic fields, starting from 2 T. The experimental results are shown in Fig. 4. The time dependence of the decay of the two-pulse (primary) photon echo was non-exponential and was approximated by the empirical Mims formula [25] used in the presence of spectral diffusion:

$$I(\tau) = I_0 e^{-2\left(\frac{\tau}{T_M}\right)^x}, \tag{1}$$

where τ is the delay time between two exciting laser pulses, the parameter x determines the form of the decay curve of the photon echo intensity, and T_M is effective phase relaxation time. An increase in the magnetic field B leads to a monotonous increase in T_M and a simultaneous decrease in the parameter x (Fig. 4). In a magnetic field 4 T, the relaxation time T_M reached $\sim 38(1)\mu\text{s}$ ($x \sim 1$) at $\mathbf{B} \parallel c$ and $\sim 31(1)\mu\text{s}$ ($x \sim 1.1$) at $\mathbf{B} \perp c$.

In sample S3, the phase relaxation time T_M was $\sim 14(1)\mu\text{s}$ at $x \sim 1.3$ in much weaker magnetic fields ($B \sim 0.5\text{T}$) compared to the case of sample S1. With an increase in the magnetic field ($\mathbf{B} \perp c$) T_M rapidly increased with a simultaneous decrease in the parameter x . So, $T_M = 54(1)\mu\text{s}$ and $x = 1.1$ at $B = 4\text{T}$. For $\mathbf{B} \parallel c$ T_M increased faster and for $B = 4\text{T}$ it was $113(3)\mu\text{s}$, but the parameter x did not change within the experimental error.

The dependence of the effective homogeneous linewidth on the magnetic field for sample S3 is shown in Fig. 5. For the S1 sample, it was possible to observe the photon echo (and, accordingly, to measure the phase relaxation time) only in magnetic fields starting from 2 T. For this reason, insufficient experimental data were obtained to

explain the dependence of the effective homogeneous width on the magnetic field as part of the model proposed below. Therefore, this dependence is given only for the S3 crystal, where the experimental data were obtained for magnetic fields from 0.5 to 4 T.

To determine the dominant mechanisms of phase relaxation, we used the approach [10,11] developed for describing the photon echo. T_M and the effective linewidth $1/\pi T_M$, respectively, can be related to the substance parameters as follows:

$$T_M(B) = \frac{2\Gamma_0}{\Gamma_{SD}R} \left(-1 + \sqrt{1 + \frac{\Gamma_{SD}R}{\pi\Gamma_0^2}} \right), \quad (2)$$

Γ_{SD} is the width of the dynamic distribution of transition frequencies due to dipole-dipole interactions. This contribution to the effective linewidth is approximately determined by the following formula:

$$\Gamma_{SD} = \frac{\pi}{9\sqrt{3}} \frac{\mu \left| |g_{|1\rangle|2\rangle}| - |g_{|3\rangle|4\rangle}| \right| |g_{env}| \mu_B^2 N}{h} \times \text{sech}^2 \left(\frac{|g_{env}| \mu_B B}{2kT} \right), \quad (3)$$

where $g_{|1\rangle|2\rangle}$ is g_{\parallel} or g_{\perp} of the ground Kramers doublet depending on the orientation of the sample in the magnetic field; $g_{|3\rangle|4\rangle}$ is the same for the doublet Γ_6^1 ($^4I_{13/2}$), $g_{env} = g_{|1\rangle|2\rangle}$, i.e. we assume that the main contribution to Γ_{SD} is made by spin flips of impurity Er ions, and the influence of nuclear magnetic moments of Y and P is small, μ is vacuum permeability, μ_B is Bohr magneton, h is Planck's constant. N is spin density, in our case we assume that this is the density of Er ions (for S3 $N \approx 7 \cdot 10^{17} \text{ cm}^{-3}$), k is Boltzmann constant, T is temperature, R is the characteristic rate of the process of spectral diffusion, determined by the sum of the rates of up and down flip transitions of perturbed Er spins. R is the following:

$$R(B) = \alpha_D |g_{env}|^3 B^5 \coth \left(\frac{|g_{env}| \mu_B B}{2kT} \right) + \alpha_{ff} g_{env}^4 \text{sech}^2 \left(\frac{|g_{env}| \mu_B B}{2kT} \right) + R_0,$$

where the first term describes the direct one-phonon spin flip process, which often dominates at low temperatures and strong magnetic fields, α_D is a constant of this process. The second term is the average rate of spin flips, where α_{ff} is a constant depending on the crystal field and the shape of the resonance line. The second term can be significant at low magnetic fields. R_0 represents relaxation processes independent of the magnetic field (contributions of Raman transitions [26,27]). Γ_0 is the following:

$$\Gamma_0 = \frac{1}{\pi T_{|3\rangle}} + \Gamma_{SD} + \Delta\Gamma_{s|1\rangle|2\rangle} + \Delta\Gamma_{s|3\rangle|4\rangle} + \Delta\Gamma_{D|3\rangle|6\rangle}, \quad (4)$$

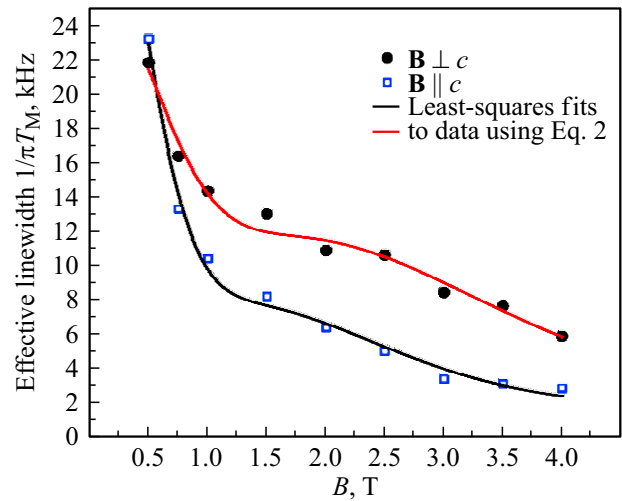


Figure 5. Dependence of the effective homogeneous linewidth of erbium ions in an $YPO_4:Er^{3+}$ crystal on the magnetic field. The blue and black symbols refer to the two S3 sample orientations in the magnetic field. Red and black curves are approximations of the results using the formula (2).

where $T_{|3\rangle}$ is the lifetime of state $|3\rangle$ and $\frac{1}{\pi T_{|3\rangle}}$ is the homogenous linewidth associated with finite state lifetime $|3\rangle$. In our case $T_{|3\rangle} \sim 5$ ms, and this homogeneous width is only ~ 64 Hz. γ_{SD} corresponds to the influence of processes of instantaneous spectral diffusion; $\Delta\Gamma_{s|1\rangle|2\rangle}$ and $\Delta\Gamma_{s|3\rangle|4\rangle}$ are broadenings caused by spin-lattice relaxation in the ground and optically excited (Γ_6^1 ($^4I_{13/2}$)) Kramers doublets, respectively. These contributions can be evaluated in the following way:

$$\Delta\Gamma_{s_l} = \frac{R(B)}{4\pi} \exp \left(-\frac{|g| \mu_B B}{2kT} \right) \text{sech} \left(\frac{|g| \mu_B B}{2kT} \right).$$

The last term

$$\Delta\Gamma_{D|3\rangle|6\rangle} = R_{|3\rangle|6\rangle} \exp \left(-\frac{\Delta_{|3\rangle|6\rangle}}{kT} \right)$$

in formula (4) corresponds to direct relaxation processes between states $|3\rangle$ and $|6\rangle$. It should be noted that the g factors $g_{|3\rangle|4\rangle}$ and $g_{|5\rangle|6\rangle}$ have different signs in two orientations of magnetic fields, $B \perp c$ and $B \parallel c$. For this reason, direct relaxation processes are possible from the $|3\rangle$ state to the $|6\rangle$ state and are prohibited to the $|5\rangle$ state. In the last term of the equation (4) $R_{|3\rangle|6\rangle}$ is the rate of direct relaxation processes between the states $|3\rangle$ and $|6\rangle$, $\Delta_{|3\rangle|6\rangle}$ is the energy difference between the states $|3\rangle$ and $|6\rangle$, and

$$\Delta_{|3\rangle|6\rangle} = \Delta_0 + 0.5(|g_{|3\rangle|4\rangle}| + |g_{|5\rangle|6\rangle}|) \mu_B B,$$

where $\Delta_0 = 10.4 \text{ cm}^{-1} = 312 \text{ GHz}$.

At the first step of approximating the experimental data $1/\pi T_M$, we used the expression for Γ_0 in the following form:

$$\Gamma_0 = \Gamma + R_{|3\rangle|6\rangle} \exp \left(-\frac{\Delta_{|3\rangle|6\rangle}}{kT} \right),$$

Parameters of the best approximation of the dependence of the effective homogeneous width on the magnetic field

Orientation of the magnetic field	Γ_0 , kHz	R_0 , kHz	α_D , Hz/T ⁵	α_{ff} , Hz
$\mathbf{B} \parallel c$	1.9 ± 0.7	5 ± 2	15 ± 4	17 ± 3
$\mathbf{B} \perp c$	2.1 ± 1.9	22 ± 6	60 ± 20	30 ± 20

where Γ is the sum of the first two terms of equation (4). Five parameters α_D , α_{ff} , Γ , R_0 , and $R_{|3\rangle|6\rangle}$ were varied. The best fit gives the value $R_{|3\rangle|6\rangle} \sim 64$ MHz, but with a large (of the value order of the parameter itself) error in determining the parameter value. This is due to the fact that at such rates of this direct relaxation process, its contribution becomes insignificant even at low magnetic fields. Thus, for $B = 0$ the value of this contribution is ~ 640 Hz, at $B = 0.5$ T $\Delta\Gamma_{D|3\rangle|6\rangle} \sim 255$ Hz and only 0.4 Hz at $B = 4$ T (at $\mathbf{B} \perp c$, when the sum of $|g_{|3\rangle|4\rangle}| + |g_{|5\rangle|6\rangle}|$ has a minimum value). Thus, the effect of the studied direct relaxation process on the linewidth can be considered insignificant. At the next stage, we varied only four parameters α_D , α_{ff} , R_0 , and Γ_0 , and for simplicity we assumed that Γ_0 does not depend on the magnitude of the magnetic field. The parameters of the best approximation are presented in the table, and the corresponding curves — in Fig. 5.

The obtained parameters α_D , α_{ff} , R_0 allow to calculate the values of $R(B)$ depending on the magnetic field and estimate the possible contribution of $\Delta\Gamma_{s|1\rangle|2\rangle}$ and $\Delta\Gamma_{s|3\rangle|4\rangle}$. Our estimates show that the sum of these contributions does not exceed 1.2 kHz and 1 Hz at $B = 0.5$ and 4 T ($\mathbf{B} \perp c$), respectively. For $\mathbf{B} \parallel c$ the sum of contributions is less than 440 and 14 Hz at $B = 0.5$ and 4 T, respectively. Thus, direct spin-lattice relaxation processes in the ground and excited Kramers doublets can be neglected.

Conclusion

Thus, for the first time, studies of the $\text{YPO}_4:\text{Er}^{3+}$ crystal were carried out by the method of primary photon echo. The largest value of the coherence time (113 μs) was obtained for the sample with the lowest impurity concentration of Er ions and for the magnetic field orientation $\mathbf{B} \parallel c$ ($B = 4$ T), i.e., for the case when the effective g factors of the ground and excited Kramers doublets have the highest values, which corresponds to the most favorable conditions for the strong polarization of the electron spins of the ensemble of Er ions. The obtained dependences of the effective homogeneous linewidth indicate that a longer phase relaxation time can be obtained in higher magnetic fields. The large value of Γ_0 can be associated with the presence of instantaneous spectral diffusion; in addition, we do not exclude the presence of additional magnetic impurities in the crystal, the appearance of which is due

to the crystal growth method and the presence of Pb ions in the high-temperature melt, which can affect the homogeneous linewidth, and this is not taken into account in the model explaining the dependence of the effective homogeneous linewidth on the magnetic field. Both of these circumstances are the subject of further research. The relatively short coherence time obtained at the optical transition puts this crystal on a par with the already well-studied oxide crystals [1,7,8], and this does not make it particularly promising for the implementation of such quantum informatics devices as, for example, quantum memory using only optical transition. However, we believe that the well spectrally resolved hyperfine structure of $^{167}\text{Er}^{3+}$ in YPO_4 can allow us to effectively redistribute the population between the hyperfine sublevels of the ground Kramers doublet (the lifetimes and coherences of which can be much higher) similarly, for example, [28] and use these sublevels for storing quantum information. It is planned to grow and study YPO_4 crystals with isotopically enriched $^{167}\text{Er}^{3+}$ ions for this.

Funding

This paper was supported by the Ministry of Science and Higher Education of the Russian Federation (Reg. № NIOKTR 121020400113-1 and FFUU-2022-0003). E.I. Baibekov thanks the Foundation for the Development of Theoretical Physics and Mathematics „BASIS“.

Conflict of interest

The authors declare that they have no conflict of interest.

References

- [1] P. Goldner, A. Ferrier, O. Guillot-Noël. *Rare earth-doped crystals for quantum information processing. Handbook on the Physics and Chemistry of Rare Earths* (Elsevier, Amsterdam, 2015), vol. 46, Ch. 267, pp. 1–78.
- [2] M. Zhong, M.P. Hedges, R.L. Ahlefeldt, J.G. Bartholomew, S.E. Beavan, S.M. Wittig, J.J. Longdell, M.J. Sellars. *Nature* **517** (7533), 177 (2015). DOI: 10.1038/nature14025
- [3] A. Ortu et al. *Nat. Mater.*, **17**(8), 671–675 (2018). DOI: 10.1038/s41563-018-0138-x
- [4] M.P. Hedges, J.J. Longdell, Y. Li, M.J. Sellars. *Nature*, **465** (2), 1052–1056 (2010). DOI: 10.1038/nature09081
- [5] L.A. Williamson, Y.-H. Chen, J.J. Longdell. *Phys. Rev. Lett.*, **113** (20), 203601 (2014). DOI: 10.1103/PhysRevLett.113.203601
- [6] K. Kutluer et al. *Phys. Rev. Lett.*, **123** (3), 030501 (2019). DOI: 10.1103/PhysRevLett.123.030501
- [7] R.M. Macfarlane. *J. Lumin.*, **100** (1–4), 1 (2002). DOI: 10.1016/S0022-2313(02)00450-7
- [8] C.W. Thiel, T. Bottger, R.L. Cone. *J. Lumin.*, **131** (3), 353 (2011). DOI: 10.1016/j.jlumin.2010.12.015
- [9] R.W. Equall, Y. Sun, R.L. Cone, R.M. Macfarlane. *Phys. Rev. Lett.*, **72** (14), 2179 (1994). DOI: 10.1103/PhysRevLett.72.2179

- [10] T. Böttger, C.W. Thiel, Y. Sun, R.L. Cone. *Phys. Rev. B*, **73** (7), 075101 (2006). DOI: 10.1103/PhysRevB.73.075101
- [11] T. Böttger, C.W. Thiel, R.L. Cone, Y. Sun. *Phys. Rev. B*, **79** (11), 115104 (2009). DOI: 10.1103/PhysRevB.79.115104
- [12] M. Rančić, M.P. Hedges, R.L. Ahlefeldt, M.J. Sellars. *Nat. Phys.*, **14** (1), 50 (2017). DOI: 10.1038/nphys4254
- [13] N. Sangouard, C. Simon, H. de Riedmatten, N. Gisin. *Rev. Mod. Phys.*, **83** (1), 33 (2011). DOI: 10.1103/RevModPhys.83.33
- [14] B. Lauritzen, J. Minář, H. de Riedmatten, M. Afzelius, N. Sangouard, Ch. Simon, N. Gisin. *Phys. Rev. Lett.*, **104** (8), 080502 (2010). DOI: 10.1103/PhysRevLett.104.080502
- [15] F. Bussi eres, Ch. Clausen, A. Tiranov, B. Korzh, V.B. Verma, S.W. Nam, F. Marsili, A. Ferrier, Ph. Goldner, H. Herrmann, Ch. Silberhorn, W. Sohler, M. Afzelius, N. Gisin. *Nat. Photon.*, **8** (10), 775 (2014). DOI: 10.1038/nphoton.2014.215
- [16] E. Saglamyurek, J. Jin, V.B. Verma, M.D. Shaw, F. Marsili, S.W. Nam, D. Oblak, W. Tittel. *Nature Photon.*, **9** (2), 83 (2015). DOI: 10.1038/nphoton.2014.311
- [17] I. Craiciu, J. Rochman, M. Lei, E. Miyazono, J.M. Kindem, J. Bartholomew, T. Zhong, A. Faraon. *Proc. SPIE*, 10933, *Advances in Photonics of Quantum Computing, Memory, and Commun. XII*, 109330Q (4 March 2019). DOI: 10.1117/12.2510217
- [18] N. Ohlsson, R.K. Mohan, S. Kr oll. *Optics Commun.*, **201** (1–3), 71 (2002). DOI: 10.1016/S0030-4018(01)01666-2
- [19] R. Kolesov et al. *Nat. Commun.*, **3** (1), 1029, (2012). DOI: 10.1038/ncomms2034
- [20] M. Raha, S. Chen, C.M. Phenicie et al. *Nat Commun.*, **11** (1), 1605 (2020). DOI: 10.1038/s41467-020-15138-7
- [21] J.M. Kindem, A. Ruskuc, J.G. Bartholomew et al. *Nature*, **580** (7802), 201–204 (2020). DOI: 10.1038/s41586-020-2160-9
- [22] M.N. Popova, S.A. Klimin, S.A. Moiseev, K.I. Gerasimov, M.M. Minnegaliev, E.I. Baibekov, G.S. Shakurov, M. Bettinelli, M.C. Chou. *Phys. Rev. B*, **99** (23), 235151 (2019). DOI: 10.1103/PhysRevB.99.235151
- [23] S.A. Klimin, D.S. Pytalev, M.N. Popova, B.Z. Malkin, M.V. Vanyunin, S.L. Korableva. *Phys. Rev. B*, **81** (4), 1 (2010). DOI: 10.1103/PhysRevB.81.045113
- [24] G.M. Wang, R.W. Equall, R.L. Cone, M.J.M. Leask, K.W. Godfrey, F.R. Wondre. *Opt. Lett.*, **21** (11), 818 (1996). DOI: 10.1364/OL.21.000818
- [25] W.B. Mims. *Phys. Rev.*, **168** (2), 370 (1968). DOI: 10.1103/PhysRev.168.370
- [26] D.E. McCumber, M.D. Sturge. *J. Appl. Phys.*, **34** (6), 1682 (1963). DOI: 10.1063/1.1702657
- [27] R. Orbach. *Proc. Roy. Soc. London Ser. A*, **264** (1319), 458 (1961). DOI: 10.1098/rspa.1961.0211
- [28] J.S. Stuart, M.M. Hedges, R. Ahlefeldt, M. Sellars. *Phys. Rev. Res.*, **3** (3), L032054 (2021). DOI: 10.1103/PhysRevResearch.3.L032054

Translated by E.Potapova